THE JOURNAL OF BIOLOGICAL CHEMISTRY VOL. 288, NO. 12, pp. 8313–8320, March 22, 2013

The Allosteric Mechanism Induced by Protein Kinase A (PKA) Phosphorylation of Dematin (Band 4.9)*

Received for publication, November 21, 2012, and in revised form, January 15, 2013 Published, JBC Papers in Press, January 25, 2013, DOI 10.1074/jbc.M112.438861

Lin Chen[‡1,2], **Jeffrey W. Brown**[‡1,3], **Yee-Foong Mok**[§], **Danny M. Hatters**[§], **and C. James McKnight**[‡4]

From the [‡]*Department of Physiology and Biophysics, Boston University School of Medicine, Boston, Massachusetts 02118 and* [§]*Department of Biochemistry and Molecular Biology and Bio21 Molecular Science and Biotechnology Institute, University of Melbourne, Parkville, Victoria 2010, Australia*

Background: Protein kinase A regulates the stability of the erythrocyte via phosphorylation of the cytoskeletal protein dematin (band 4.9).
Results: We present an experimentally derived allosteric mechanism for PKA phosphorylation of dematin.
Conclusion: A phosphorylation mimicking mutation in the folded headpiece causes it to bind to the natively unfolded core domain of dematin.
Significance: PKA phosphorylation of dematin represents a novel conformational switch.

Dematin (band 4.9) is an F-actin binding and bundling protein best known for its role within red blood cells, where it both stabilizes as well as attaches the spectrin/actin cytoskeleton to the erythrocytic membrane. Here, we investigate the structural consequences of phosphorylating serine 381, a covalent modification that turns off F-actin bundling activity. In contrast to the canonical doctrine, in which phosphorylation of an intrinsically disordered region/protein confers affinity for another domain/protein, we found the converse to be true of dematin: phosphorylation of the well folded C-terminal villin-type headpiece confers affinity for its intrinsically disordered N-terminal core domain. We employed analytical ultracentrifugation to demonstrate that dematin is monomeric, in contrast to the prevailing view that it is trimeric. Next, using a series of truncation mutants, we verified that dematin has two F-actin binding sites, one in the core domain and the other in the headpiece domain. Although the phosphorylation-mimicking mutant, S381E, was incapable of bundling microfilaments, it retains the ability to bind F-actin. We found that a phosphorylation-mimicking mutant, S381E, eliminated the ability to bundle, but not bind F-actin filaments. Lastly, we show that the S381E point mutant caused the headpiece domain to associate with the core domain, leading us to the mechanism for cAMP-dependent kinase control of dematin's F-actin bundling activity: when unphosphorylated, dematin's two F-actin binding domains move independent of one another permitting them to bind different F-actin filaments. Phosphorylation causes these two domains to associate, forming a compact structure, and sterically eliminating one of these F-actin binding sites.

Dematin, also known as Band 4.9, is a 43–46-kDa F-actin binding and bundling protein, found in several tissue types throughout the human body (1–3). It is best known for its role within the red blood cell, where it has been localized to the junctional complex (4), a macromolecular association of at least seven different proteins that surround a short actin protofilament. These junctional complexes act as both the central hub for the approximately hexagonal spectrin lattice (5, 6) as well as a point of attachment between the cytoskeleton and the erythrocytic membrane. Relative to wild-type, dematin headpiece knock-out mice have fragile, spherocytic red blood cells, which results in a compensated anemia (7). This phenotype as well as subsequent analysis (7–9) suggests that dematin is involved in anchoring the actin-spectrin cytoskeleton to the underlying membrane. In humans, this interaction is mediated through the direct association of dematin with GLUT-1, an intrinsic membrane protein (9). More recently, dematin has also been shown to stabilize the association between actin and spectrin, and this activity is turned off by PKA phosphorylation (10). The stabilizing effect that dematin has on the cytoskeleton is specifically targeted by *Plasmodium* spp., the pathogens causing malaria, by sequestering dematin within their parasitophorous vacuole (11). Corroborating this mechanism is the observation that the efficiency of *P. falciparum* infection positively correlates with cAMP levels (12), which inactivates dematin via PKA. Thus, inhibition of dematin contributes to the pathogenesis of malarial infection.

In addition to its functionality within red blood cells, dematin also plays important roles within several nucleated cell types, which are described below; however, it is less clear whether these functions stem directly from its influence on the cytoskeleton or indirectly through modulating cell signaling pathways (3, 13). The dematin headpiece knock-out mouse exhibits coarse, wiry hair, and an absence of eyebrows (7, 8, 14). In humans, an autosomal dominant disease, Marie Unna hereditary hypotrichosis, has a very similar phenotype and results from the disruption of 8p21, the genetic locus of dematin (15). Further, the absence of dematin may also represent a significant step along the progression to prostate cancer. This is supported

* This work was supported, in whole or in part, by National Institutes of Health Grant GM62886 (to C. J. M.). This work was also supported by a Boston University graduate student research fellowship (to J. W. B.).
[1] Both authors contributed equally to this work.
[2] Present address: BIOK&KM, Sand Hill Rd., No. 853 Jiangyin City, Jiangsu Province, China.
[3] Present address: Internal Medicine Residency Program, University of Pittsburgh Medical Center, Pittsburgh, PA 15213.
[4] To whom correspondence should be addressed: 700 Albany St., W302, Boston, MA 02118. Fax: 617-638-4041; E-mail: cjmck@bu.edu.

by the dematin gene being frequently deleted in prostate cancer (16) and, when reintroduced, it reverts the overt cancerous phenotype to that of normal prostate cells (17).

The primary sequence of dematin can be divided into two regions: an N-terminal core domain and a C-terminal "villin-type" headpiece domain (Fig. 1). The headpiece domain is well folded (18, 19), whereas the core domain is intrinsically disordered (20). Further, we have also shown that these two domains move independently of one another in solution (20). The lack of secondary structure in the core domain is likely the result of a high proline content (10.7%) as well as a preponderance of charged residues (122/381), both of which are characteristic of intrinsically disordered proteins (21, 22).

With respect to dematin's F-actin binding and bundling activity, the literature has focused almost exclusively on its headpiece domain. Several studies have shown that dematin headpiece binds F-actin (19, 23, 24), as is true of nearly all headpiece domains. A unique feature of dematin headpiece is that the third to last residue is a serine (S381; glycine in all other headpiece domains) and that phosphorylation of this residue reversibly inhibits bundling activity of the full-length construct (25); however, counterintuitively, it has also been shown that phosphorylation does not inhibit the F-actin binding activity of dematin headpiece in isolation (23). In this report, we study the dynamic interaction between the dematin headpiece and the natively unfolded core domain and demonstrate that this association is controlled by PKA phosphorylation and is responsible for regulating dematin's F-actin bundling activity.

EXPERIMENTAL PROCEDURES

Cloning, Expression, and Purification—All constructs displayed in Fig. 1 were created from the parent construct, rD-His, (pGEX-2T vector, described in ref. 20), using QuikChange® site directed mutagenesis. These constructs possess a cleavable N-terminal GST tag as well as a C-terminal His^6 tag, which were used to purify the proteins from the soluble supernatant. The His^6 tag (or any C-terminal tag) overlies the F-actin binding surface of the headpiece domain (23) and eliminates this activity, therefore, the C-terminal His^6 tag was not present in any construct used in experiments involving F-actin. Lastly, we used a phosphorylation-mimicking serine-to-glutamate (S381E) point mutant instead of directly phosphorylating the protein because even trace amounts of nonphosphorylated protein would give false positive results in the actin bundling assays. We have previously demonstrated that this point mutation very closely mimics the conformational changes within dematin headpiece that occur subsequent to phosphorylation (19), and in this report, we will demonstrate that it also reproduces the functionality.

Escherichia coli strain BL21 or BL21(DE3) cells (Novagen) were transformed with the appropriate plasmid and grown in LB medium to a cell density of ~0.6–0.8 (A_{600}). The cells were then induced for 4 h by the addition of 0.8 mM isopropyl-1-thio-β-D-galactoside. Isotopically enriched (^{15}N) proteins were obtained in a similar fashion except M9 minimal medium containing ^{15}N-ammonium chloride was used in lieu of rich medium (26).

Cell pellets were thawed in lysis buffer (10 mM phosphate, pH 7.0, 200 mM NaCl, 1 mg/ml lysozyme, 1 mM phenylmethylsulfonylfloride (PMSF), 1 mM EDTA, and either 5 mM β-mercaptoethanol or 0.5 mM DTT as reducing agents). These solutions were sonicated for 2 min on ice and centrifugally cleared. Supernatants were applied to glutathione-Sepharose 4B (Amersham Biosciences). The protein bound to the column was washed extensively with ATP buffer (10 mM phosphate, pH 7.0, 200 mM NaCl, 5 mM ATP, 5 mM $MgCl_2$, 1 mM sodium azide, 0.5 mM DTT) at room temperature to remove *E. coli* DnaK, which tightly associates with the intrinsically disordered core domain. The column was then transferred to 4 °C and equilibrated with cleavage buffer (10 mM phosphate, pH 7.0, 200 mM NaCl, 0.5 mM DTT, 1 mM sodium azide). GST fusion proteins were obtained at this point by the addition of glutathione elution buffer (50 mM Tris, pH 8.0, 5 mM reduced glutathione, 0.5 mM DTT). Constructs with the GST tag removed were collected directly off the column by on-column cleavage.

For tD and tD-S381E, the protein bound to the column was incubated with 50 units of thrombin (Amersham Biosciences) for 0.5 h at room temperature, after which, the elution was passed through *p*-aminobenzamidine-agarose (Sigma) to remove the protease. For rD and rD-Core constructs, 80 units of PreScission protease (Amersham Biosciences) was added, and the mixture was incubated for 4 h at 4 °C prior to elution. For those constructs, which contain a C-terminal 6x-His tag, the elution in 10 mM phosphate, pH 8.0, 300 mM NaCl, 10 mM imidazole, 0.5 mM DTT was slowly passed over pre-equilibrated nickel-nitrilotriacetic acid-agarose (Qiagen), and the bound proteins were eluted with a stepwise increase of imidazole (10–250 mM).

Actin was obtained from chicken pectoral muscle and purified from acetone powder using standard procedures (27). Prior to polymerization, the concentration of actin was determined by absorbance at 290 nm using an extinction coefficient of 26,640 $M^{-1}\cdot cm^{-1}$.

Analytical Ultracentrifugation—For sedimentation velocity analysis, solutions of dematin (30 μM) were added to double-sector epon-filled centerpieces and analyzed with an XL-I analytical ultracentrifuge at 20 °C (Beckman Coulter, Fullerton, CA). Radial absorbance scans (280 nm) were collected at a rotor speed of 40,000 rpm with radial increments of 0.003 cm in continuous scanning mode. The sedimenting boundaries were fitted to a model describing the sedimentation of a distribution of sedimentation coefficients, which were converted to mass units, c(M), using the program SEDFIT (28). Data were fitted using a regularization parameter of $p = 0.95$, floating frictional ratios and with 200 sedimentation coefficient increments in the range of 0.5–10 S. Partial specific volumes were calculated based on amino acid composition, and buffer densities were calculated from composition using SEDNTERP (John Philo, Thousand Oaks, CA). For the fitting to a single sedimenting species, masses were fixed as monomers, and the best fit sedimentation coefficients were analyzed by Monte Carlo analysis (1000 simulations) to obtain confidence intervals.

For sedimentation equilibrium experiments, samples were loaded into 6-sector epon-filled centerpieces at a concentration of 30 μM and centrifuged at rotor speeds of 10,000 rpm at 20 °C

until equilibrium (approximately 48 h), as assessed by the overlapping of scans taken 5 h apart. Radial scans were taken at a wavelength of 280 nm and increments of 0.001 cm in step mode. Samples were then centrifuged at 15,000 rpm for another 15 h until equilibrium was attained as indicated by overlapping scans taken at 5-h intervals. Data were analyzed in the software SEDPHAT and fitted globally for the two speeds to a model describing a single species (29) using the partial specific volume, buffer density and protein extinction coefficients calculated above with SEDNTERP.

Actin Sedimentation Assays—Increasing concentrations of pre-spun dematin stock solutions were incubated with F-actin for 1 h at 4 °C. The solutions were then spun for 1 h at 100,000 × g. The supernatant was removed and the pellets were solubilized overnight in SDS-PAGE loading buffer and electrophoresed through 12.5% SDS-polyacrylamide gels. F-actin sedimentation assays for isolated dematin headpiece constructs were performed and quantitated with reverse phase high performance liquid chromatography as previously described (24, 30).

Actin Bundling Assay—F-actin was incubated with dematin constructs at a 1:1, weight ratio (0.2 mg/ml) at 4 °C. The solutions were placed onto carbonized copper grids for 1 min, washed, and stained with 1% uranyl acetate. All samples were imaged with a Philips CM12 transmission electron microscope at 45,000× magnification under minimal dose conditions. The film was processed and digitized on a Creo IQ Smart2 Scanner (Global Imaging) at 1270 dpi.

Two-dimensional Nuclear Magnetic Resonance (NMR) Spectroscopy—^{1}H-^{15}N heteronuclear single quantum coherence (HSQC)[5] spectra were acquired at 20 °C on a Bruker DMX500 spectrometer. Solutions contained either rD, rD-S381E, tD, or tD-S381E (~25–50 μM) in 10 mM phosphate, pH 7.0, 200 mM NaCl, and 10% D_2O. Sodium 3-trimethylsilyltetradeuteropropionate (0.1 mM) was used as a chemical shift reference. The data were collected as 256 increments of 2048 data points with 128 scans per increment.

Molecular Modeling—The molecular surfaces of actin filaments (orange) were calculated from the atomic coordinates of actin (31) with the program Chimera (32) and exported to POV-RAY for further modeling (1 angstrom per POV-RAY unit) (33). Dematin was modeled as a blue prolate ellipsoid (core domain) tethered to a green sphere (headpiece) by a black linker region. The molecular size of each domain in dematin was computed from their molecular mass (35 and 10 kDa, respectively) using a value of 0.84 Da/Å^3 (34). Molecular models were rendered with POV-RAY (33).

RESULTS

Dematin Is a Monomeric Protein—Dematin has long been believed to be a trimeric protein; however, this statement was predicated only on a pseudo-3-fold appearance in rotary shadowed electron micrographs (35) and copper-phenanthroline catalyzed cysteine cross-linking experiments (36). Although we are able to reproduce these disulfide cross-linked multimers under oxidizing conditions as might be expected of any protein with a free thiol, we have been unable to cross-link them under reducing conditions with typical reagents like glutaraldehyde (data not shown). To gain a more precise view of the oligomeric status of dematin under the reducing conditions expected within the erythrocyte, we performed analytical ultracentrifugation of four constructs: (1) rD-His (core and the headpiece domain), (2) rD-S381E-His (core and the "phosphorylated" headpiece domain), (3) rD-Core-His (core domain), and (4) tD (truncated core domain and the headpiece), which are schematically represented in Fig. 1. First, we performed sedimentation velocity experiments and fitted the data to a continuous size distribution (c(M)) model (37) (Fig. 2), which produced fits indicating a monodisperse oligomeric state for each construct that was most consistent with a monomer (Fig. 2, *A* and B). To rule out possible weak oligomerization, which may not be evident by sedimentation velocity experiments, we also performed sedimentation equilibrium experiments (Fig. 2*C*). The equilibrium data, collected at two speeds, globally fitted best to models describing a monomer, which confirmed the velocity data for an absence of apparent oligomerization. Collectively, these data indicated that dematin was monomeric under these experimental conditions, which negates the current mechanism by which dematin bundles actin filaments (36, 38) as this model assumed that dematin was trimeric.

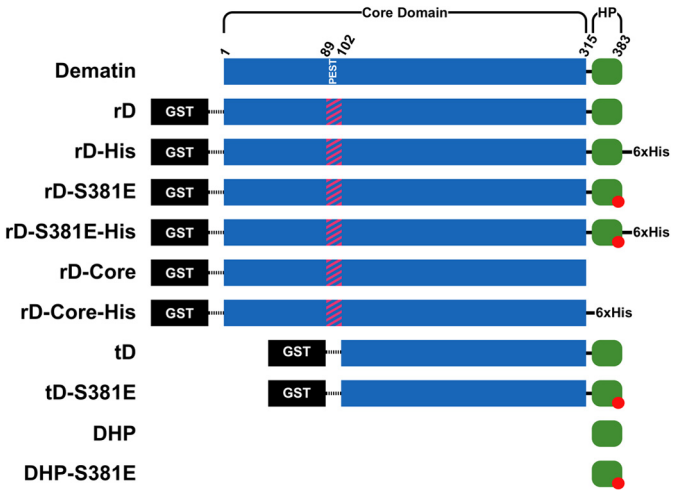

FIGURE 1. **Schematic representation of the dematin constructs used in the work.** Dematin consists of two domains, an intrinsically disordered core domain (residues 1–315; *blue*) and a headpiece domain (residues 315–383; *green*). Within the core domain there exists a PEST sequence (residues 89–102), which when present results in significant intracellular degradation. In the series of constructs called "rD" (PEST-*r*eplaced *D*ematin) the PEST residues were mutated as previously described (20). In another two constructs called "tD" (*t*runcated *D*ematin), the residues prior to and including the PEST sequence were omitted from the transcript. All constructs were expressed as *cleavable* GST-fusion proteins, some of which also contain C-terminal His[6] tags.

Both Dematin Headpiece and the Core Domain Bind F-actin—It is well established that dematin headpiece exhibits significant affinity for F-actin (23, 24); however, there also exists evidence that the core domain may also exhibit this activity (25, 38). As we have demonstrated that dematin is monomeric under reducing conditions, it follows that each protein must possess two F-actin binding sites to cross-link actin filaments. To test this hypothesis, we assayed a number of constructs for F-actin binding activity via F-actin sedimentation analysis (Fig. 3). The headpiece-containing constructs, rD and tD, clearly bind in this

[5] The abbreviation used is: HSQC, heteronuclear single quantum coherence.

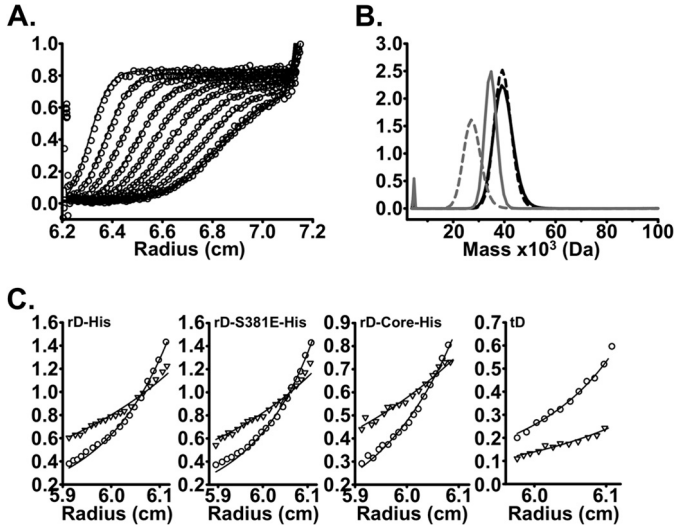

FIGURE 2. **Sedimentation analysis of dematin.** Each dematin construct (30 μM) was subjected to sedimentation velocity analysis in an analytical ultracentrifuge. *A*, representative experimental sedimenting concentration boundaries (circles) for rD-His, with the fits to the sedimentation model, c(s), shown as solid lines. *B*, mass distribution plot for dematin derived from fitting experimental data from sedimentation velocity experiments to a c(M) model. Plots are shown for rD-His (*black solid line*), rD-S381E-His (*black dashed line*), rD-core-His (*gray solid line*) and tD (*gray dashed line*). *C*, each dematin construct (30 μM) was also subjected to sedimentation equilibrium analysis at two different speeds in an analytical ultracentrifuge. Experimental concentration boundaries are shown for dematin after equilibrium has been reached at 10,000 rpm (*triangles*) and 15,000 rpm (*circles*), with the fits to a single species equilibrium model shown as *solid lines*. The fitted weight-average molecular masses were 42,312 Da for rD-His, 43,348 Da for rD-S381E-His, 38,360 Da for rD-Core-His and 34,809 Da for tD (theoretical molecular masses are 43,671 Da, 43,713 Da, 35,767 Da, and 31,808 Da for the four constructs, respectively).

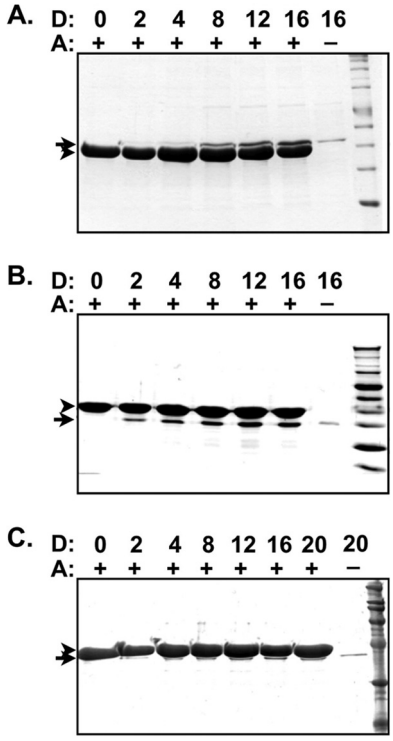

FIGURE 3. **F-actin sedimentation analysis.** SDS-PAGE displaying the pellets from an F-actin sedimentation assay performed between actin (22 μM) and a variable concentration (0–20 μM) of each of the following dematin constructs (*A*) rD (PEST-replaced), (*B*) tD (truncated), and (*C*) rD-Core-His (core domain of PEST-replaced). The *arrowhead* indicates actin, whereas the *arrow* indicates the dematin construct, whose F-actin binding activity is being tested.

qualitative assay. The core domain in isolation also binds F-actin in this assay (Fig. 3*C*), which is in accord with the results of Chishti *et al.*, 1988 (25) and Azim *et al.*, 1995 (38), but with much lower affinity than the headpiece-containing constructs.

Dematin (rD) but Not Phosphorylated Dematin (rD-S381E) Bundles Microfilaments—Because our data indicated that dematin is monomeric and has two F-actin binding sites, we hypothesized microfilament bundling activity must arise from this multivalency within a single polypeptide chain (Fig. 2). To test this hypothesis, we incubated both rD as well as several truncated dematin constructs with F-actin and assayed each for bundling activity via negative-stain electron microscopy (Fig. 4). We found that only rD, which contains both the native, unmodified headpiece domain as well as the core domain, could bundle microfilaments.

Previous studies have demonstrated that phosphorylation of serine 381 eliminates the F-actin bundling activity of dematin (25, 36). We have previously shown that the phosphorylation mimicking mutant (S381E) very closely reproduces the conformational changes that occur secondary to phosphorylation (19), and, in Fig. 4*D*, we demonstrate that this modification also eliminates F-actin bundling activity. However, counterintuitively we found that the S381E mutation does not change the F-actin *binding* activity of dematin headpiece in isolation (Fig. 5*A*) (23, 38).

Phosphorylation Results in a Compact Quaternary Structure—Because phosphorylation does not change the F-actin binding activity of dematin headpiece in isolation, we hypothesized that the loss of F-actin bundling activity could be explained by a phosphorylation induced conformational change. To this end, we determined the hydrodynamic properties of rD-His and rD-S381E-His from the data presented in Fig. 2*A*. We fitted these data to a model assuming a single sedimenting species of the monomeric mass (fixed), which is validated by the c(s) analysis and equilibrium data indicating each protein was entirely monomeric (Fig. 2, *B* and C). This analysis provided excellent fits with the generated sedimentation coefficients of $s = 2.361$ S (95% CI: 2.354 S to 2.369 S) for the rD domain and $s = 2.379$ S (95% CI: 2.367 S to 2.390 S) for the S381E mutant (Fig. 6*A*). These values correspond to frictional ratios (f/f_0) of 1.885 (95% CI: 1.879 to 1.891) and 1.872 (95% CI: 1.863 to 1.882) (Fig. 6*B*). Because f/f_0 reports on the level of asymmetry (higher values represent greater asymmetry), these results suggest that the S381E mutant is more compact than the wild-type protein.

Phosphorylation Causes the Headpiece to Associate with the Core Domain—The ^{1}H-^{15}N HSQC NMR spectrum of dematin headpiece exhibited significant peak dispersion, which is characteristic of a well folded protein (18, 19). In contrast, the core domain exhibited very little peak dispersion (Fig. 7*A*), consistent with it being intrinsically disordered (19). Furthermore, as we have previously reported, it is also missing ~180 backbone amide peaks, whose absence can be attributed to extreme broadening due to fast T_2-relaxation arising from either the slow correlation (tumbling) time of the large core domain or intermediate exchange (20).

In Fig. 7, we compare the ^{1}H-^{15}N HSQC spectra of rD-His, rD-S381E-His, tD, and tD-S381E-His. We observe both the res-

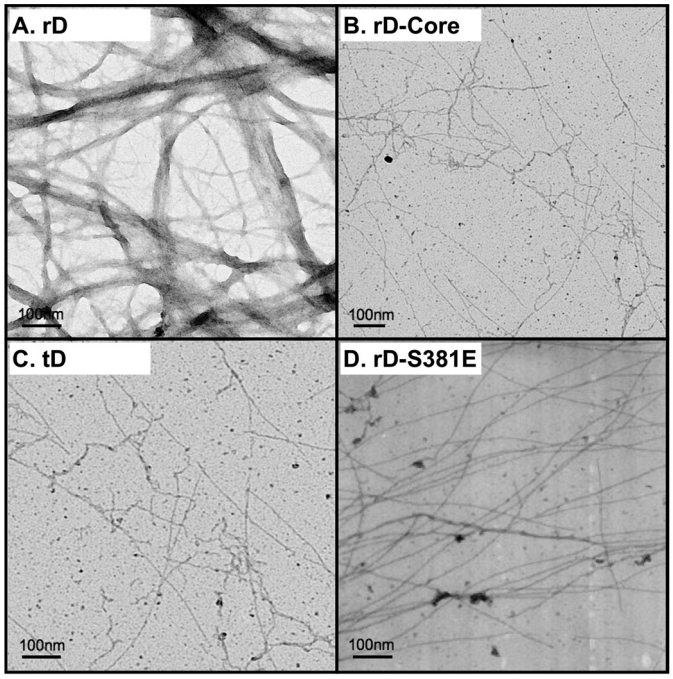

FIGURE 4. **Both the core and the native, unphosphorylated headpiece domain are required to bundle microfilaments.** Negatively stained electron micrographs display the gross organization of actin microfilaments when incubated with a 1:1 weight ratio of either (*A*) rD (PEST-replaced dematin), (*B*) rD-Core (core domain of PEST-replaced dematin), (*C*) tD (truncated dematin), or (*D*) rD-S381E (S381E point mutant of PEST-replaced dematin).

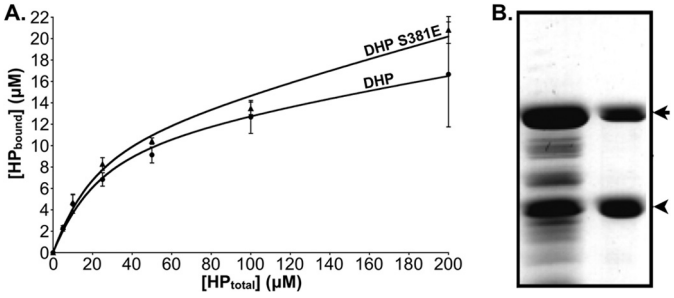

FIGURE 5. **The S381E point mutation does not affect F-actin binding activity.** *A*, F-actin binding curves of wild-type dematin headpiece and the S381E point mutant quantitated via UV absorption (A_{220}) of reverse-phase HPLC separated proteins (22). The refined dissociation constant (K_d) was 15.1 μM and 12.4 μM, and nonspecific binding was 3.1% and 5.1%, for wild-type and DHP S381E, respectively. *B*, SDS-PAGE gel displaying both the supernatant (S) and pellet (P) of an F-actin sedimentation assay performed with an equimolar (22 μM) solution of F-actin and GST-rD-S381E. The *arrow* denotes GST-rD-S381E, whereas the *arrowhead* points to actin. Note that the impurities seen in the supernatant fraction are from proteolytic cleavage between the N-terminal GST tag used to purify this sample and the C-terminal headpiece domain and do not bind F-actin. Only the full-length construct containing the headpiece domain binds tightly in this stringent assay.

onances corresponding to the natively unfolded core domain as well as the headpiece domain in all spectra except for that of rD-S381E-His, where the amide peaks arising from the headpiece domain are noticeably absent (Fig. 7*B*). The lack of signal from the headpiece domain can only be explained by an interaction with the large core domain, which will result in the headpiece assuming the fast T_2 relaxation time of the core domain and subsequent loss of its NMR signal. This phosphorylation dependent association between the core domain and the headpiece is schematically represented in Fig. 8. This mechanism is consistent with analytical ultracentrifugation data, which demonstrated that the S381E mutation results in a less asymmetric, more compact quaternary structure.

DISCUSSION

In this report, we investigated the role of dematin natively unfolded core domain with respect to its F-actin binding and bundling activity. Our results demonstrate that similar to other monomeric F-actin-binding proteins like fimbrin (39) or villin (40), dematin possesses two F-actin binding sites within a single polypeptide: one in the core domain and the other in the headpiece domain. Although the unphosphorylated headpiece domain is covalently tethered to the core domain by the peptide backbone, our NMR analysis demonstrates that their molecular motions are independent of one another. This freedom permits dematin headpiece to interact with a different actin filament than the core domain, forming parallel arrays of actin microfilaments called bundles (Fig. 8*C*).

In addition to endowing dematin with a second F-actin binding site and thus the ability to bundle microfilaments, the core domain is also essential for inhibiting this functionality subsequent to phosphorylation of the headpiece domain. The core domain is able to regulate dematin F-actin bundling activity because of the significant disparity in its affinity between the unphosphorylated and phosphorylated headpiece domain (phosphorylation begetting binding; Fig. 7*A*). In Fig. 8, we present a scaled model of dematin bound to F-actin. This level of modeling emphasizes the small size of dematin relative to actin and illustrates how the association between the headpiece and the core domain sterically prevents the protein from binding multiple actin filaments (Fig. 8).

Although we chose to use F-actin bundling activity as a prototypical reaction to demonstrate the dramatic effect that PKA phosphorylation has on the functionality of the dematin, the underlying conformational mechanism appears to control other cellular activities. For example, in mature red blood cells, which are devoid of F-actin bundles, dematin has recently been shown to stabilize the interaction between spectrin and F-actin, and this functionality is inhibited by PKA phosphorylation (10). The same molecular mechanism that we experimentally derived for actin bundling activity is easily extrapolated to tethering other ternary protein complexes linked by dematin, including spectrin and F-actin within the mature erythrocytic cytoskeleton.

In this study, we report two specific functions of dematin's intrinsically disordered core domain: (1) binding F-actin and (2) binding the "phosphorylated" headpiece domain. Although this may seem odd for a domain lacking a well defined tertiary structure, the ability to bind several different proteins is a common feature of intrinsically disordered proteins (reviewed in Ref. 41–43). In fact, with the exception of enzymatic catalysis, which is nearly always performed by proteins with a well defined tertiary structure, several advantages are conferred by intrinsic disorder. These include the ability to bind a greater number of proteins due increased malleability as well as the fact that proteins lacking a well defined structure generally exhibit a larger effective molecular interface (41–43). Furthermore, in natively unfolded proteins, the act of binding is inseparable from the folding reaction, which permits fine-tuning and high-

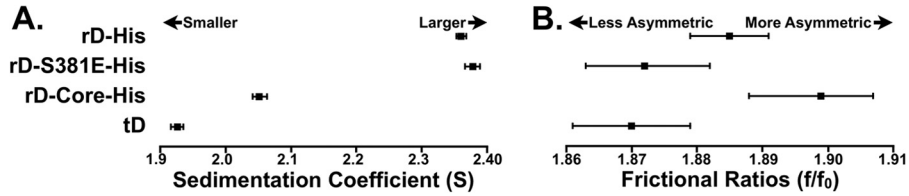

FIGURE 6. **Computed sedimentation coefficients and frictional ratios.** *A*, Plot of sedimentation coefficients (S) for rD-His, rD-S381E-His, rD-Core-His, and tD. *B*, Plot of frictional ratios (f/f_0) for rD-His, rD-S381E-His, rD-Core-His, and tD. *Error bars* in *A* and *B* indicate the 95% confidence intervals using Monte Carlo analysis.

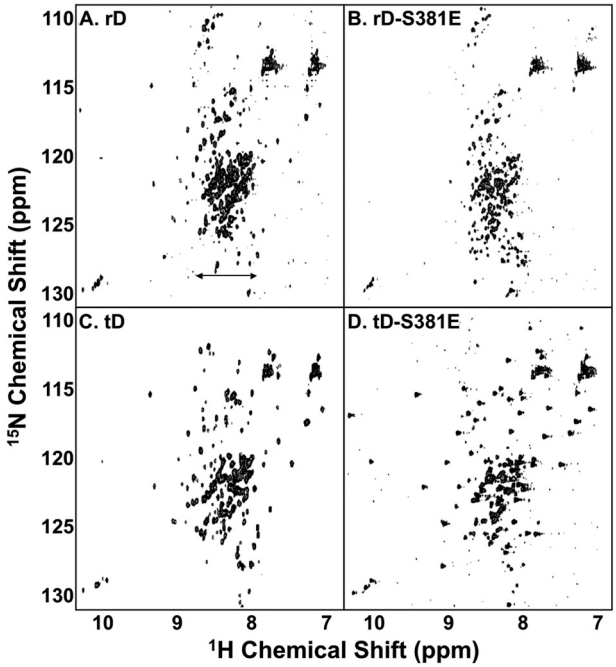

FIGURE 7. **Phosphorylation at Ser-381 causes dematin headpiece to associate with the core domain.** 500 MHz ^{15}N-HSQC NMR spectra of *A*, rD, *B*, rD-S381E, *C*, tD, and *D*, tD-S381E. Protein concentrations were 20–50 μM in 200 mM NaCl, 10 mM phosphate pH 7.0, at 20 °C with 10% D_2O. The *horizontal arrow* in *A*, denotes very small dispersion along the ^{1}H dimension arising from the similar chemical environments of the backbone amides due to the intrinsic disorder of the core domain.

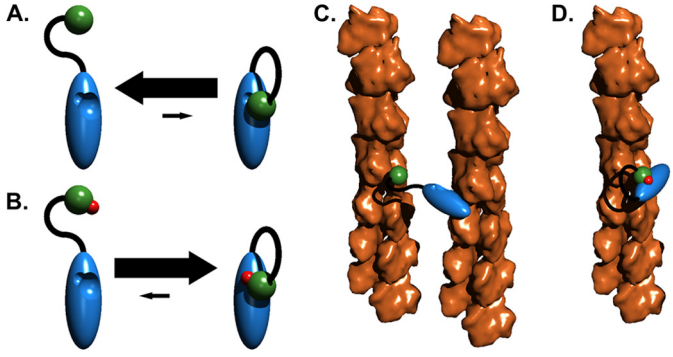

FIGURE 8. **Molecular mechanism by which phosphorylation inhibits the F-actin bundling activity of dematin.** *A*, wild-type (unphosphorylated) dematin primarily populates the "open state," a quaternary structure in which the molecular motion of dematin headpiece is largely independent of the core domain. *B*, in contrast, the phosphorylated version favors the "closed state", in which the phosphorylated headpiece is bound to the core domain. *C*, in the open state, dematin is able to bind two microfilaments and thus form bundles; however, subsequent to phosphorylation (*D*, closed state) dematin is only able to bind a single microfilament.

specificity by balancing the enthalpic energy gained through binding with the loss of entropy due to folding (41–43). This high-specificity typically comes at the cost of low affinity; however, in our system, this would be offset by the covalent attachment between the two domains that greatly increases their effective concentration for one another. This process might be an important aspect of the core domain's ability to discriminate between the dematin headpiece with an uncharged hydroxyl (Ser-381) relative to a negatively charged phosphate (that we mimicked with Glu-381) at a single position within dematin headpiece domain.

A significant difference between dematin and nearly all other phosphorylation-controlled conformational changes is that in dematin, phosphorylation of the well folded villin-type headpiece domain confers affinity for the intrinsically disordered core domain. This is the converse of the canonical reaction in which phosphorylation of an intrinsically disordered domain creates affinity for either a well structured domain or another intrinsically disordered domain (41–43).

Although we have reiterated that the N-terminal core domain of dematin is intrinsically disordered, it should not be assumed this is meant to denote that this domain is a randomly ordered linear chain of amino acids because, if this were true, we would have expected to observe all amide peaks in our NMR spectra due to their unrestrained motion (Fig. 7) (20). Instead, dematin likely exists as an ensemble of several metastable states each devoid of significant secondary structural elements but possessing some degree of order. This idea is corroborated by a multiple sequence alignment of dematin from several mammalian species, which reveals an extremely high degree of conservation (>94% identity). Furthermore, the intrinsically disordered core domain of dematin actually has another homolog, limatin (44), which exhibits ~36 and 48% identity with the core domain and entire sequence of dematin, respectively.

In summary, we present the molecular mechanism by which PKA phosphorylation regulates the functionality of dematin, using F-actin bundling activity as the prototypical reaction. When unphosphorylated, dematin's two F-actin binding domains move independently of one another permitting them to bind different F-actin filaments. Phosphorylation causes these two domains to associate, sterically eliminating one of these F-actin binding sites. Contrary to the canonical mechanism, in which phosphorylation of intrinsically disordered regions endows a protein with new binding affinities, we found the converse to be true of dematin: phosphorylation of the well folded villin-type headpiece domain conferred affinity for the intrinsically disordered core domain. Our results bring forth the notion that there are essential phosphorylation sites within well folded regions that will be systematically missed by *in silico* algorithms because they assume intrinsic disorder and therefore use only local sequence information. The presence of secondary structure in a globular protein obscures very local

sequence and thus to identify phosphorylation sites like that in dematin headpiece would require three-dimensional structural information.

Acknowledgments—We thank Zhenghui G. Jiang for assistance with electron microscopy and Esther Bullitt for careful reading and helpful comments on the manuscript.

REFERENCES

1. Faquin, W. C., Husain, A., Hung, J., and Branton, D. (1988) An immunoreactive form of erythrocyte protein 4.9 is present in non-erythroid cells. *Eur. J. Cell Biol.* **46,** 168–175
2. Rana, A. P., Ruff, P., Maalouf, G. J., Speicher, D. W., and Chishti, A. H. (1993) Cloning of human erythroid dematin reveals another member of the villin family. *Proc. Natl. Acad. Sci. U.S.A.* **90,** 6651–6655
3. Mohseni, M., and Chishti, A. H. (2008) The headpiece domain of dematin regulates cell shape, motility, and wound healing by modulating RhoA activation. *Mol. Cell. Biol.* **28,** 4712–4718
4. Derick, L. H., Liu, S. C., Chishti, A. H., and Palek, J. (1992) Protein immunolocalization in the spread erythrocyte membrane skeleton. *Eur. J. Cell Biol.* **57,** 317–320
5. Byers, T. J., and Branton, D. (1985) Visualization of the protein associations in the erythrocyte membrane skeleton. *Proc. Natl. Acad. Sci. U.S.A.* **82,** 6153–6157
6. Nans, A., Mohandas, N., and Stokes, D. L. (2011) Native ultrastructure of the red cell cytoskeleton by cryoelectron tomography. *Biophys. J.* **101,** 2341–2350
7. Khanna, R., Chang, S. H., Andrabi, S., Azam, M., Kim, A., Rivera, A., Brugnara, C., Low, P. S., Liu, S. C., and Chishti A. H. (2002) Headpiece domain of dematin is required for the stability of the erythrocyte membrane. *Proc. Natl. Acad. Sci. U.S.A.* **99,** 6637–6642
8. Chen, H., Khan, A. A., Liu, F., Gilligan, D. M., Peters, L. L., Messick, J., Hacshek-Hock, W. M., Li, X., Ostafin, A. E., and Chishti, A. H. (2007) Combined deletion of mouse dematin-headpiece and β-adducin exerts a novel effect on the spectrin-actin junctions leading to erythrocyte fragility and hemolytic anemia. *J. Biol. Chem.* **282,** 4124–4135
9. Khan, A. A., Hanada, T., Mohseni, M., Jeong, J. J., Zeng, L., Gaetani, M., Li, D., Reed, B. C., Speicher, D. W., and Chishti, A. H. (2008) Dematin and adducin provide a novel link between the spectrin cytoskeleton and human erythrocyte membrane by directly interacting with glucose transporter-1. *J. Biol. Chem.* **283,** 14600–14609
10. Koshino, I., Mohandas, N., and Takakuwa, Y. (2012) Identification of a novel role for dematin in regulating red cell membrane function by modulating spectrin-actin interaction. *J. Biol. Chem.* **287,** 35244–35250
11. Lalle, M., Currà, C., Ciccarone, F., Pace, T., Cecchetti, S., Fantozzi, L., Ay, B., Breton, C. B., and Ponzi, M. (2011) Dematin, a component of the erythrocyte membrane cytoskeleton, is internalized by malaria parasite and associates with Plasmodium 14–3-3. *J. Biol. Chem.* **286,** 1227–1236
12. Harrison, T., Samuel, B. U., Akompong, T., Hamm, H., Mohandas, N., Lomasney, J. W., and Haldar, K. (2003) Erythrocyte G protein-coupled receptor signaling in malarial infection. *Science* **301,** 1734–1736
13. Lutchman, M., Kim, A. C., Cheng, L., Whitehead, I. P., Oh, S. S., Hanspal, M., Boukharov, A. A., Hanada, T., and Chishti, A. H. (2002) Dematin interacts with Ras-guanine nucleotide exchange factor Ras-GRF2 and modulates mitogen-activated protein kinase pathways. *Eur. J. Biochem.* **269,** 638–649
14. Mohseni, M., and Chishti, A. H. (2008) Erythrocyte dematin is a candidate gene for Marie Unna hereditary hypotrichosis and related hair loss disorders. *Am. J. Hematol.* **83,** 430–432
15. Sreekumar, G. P., Roberts, J. L., Wong, C. Q., Stenn, K. S., and Parimoo, S. (2000) Marie Unna hereditary hypotrichosis gene maps to human chromosome 8p21 near hairless. *J. Invest. Dermatol.* **114,** 595–597
16. Vocke, C. D., Pozzatti, R. O., Bostwick, D. G., Florence, C. D., Jennings, S. B., Strup, S. E., Duray, P. H., Liotta, L. A., Emmert-Buck, M. R., and Linehan, W. M. (1996) Analysis of 99 microdissected prostate carcinomas reveals a high frequency of allelic loss on chromosome 8p12-21. *Cancer Res.* **56,** 2411–2416
17. Lutchman, M., Pack, S., Kim, A. C., Azim, A., Emmert-Buck, M., van Huffel, C., Zhuang, Z., and Chishti, A. H. (1999) Loss of heterozygosity on 8p in prostate cancer implicates a role for dematin in tumor progression. *Cancer Genet. Cytogenet.* **115,** 65–69
18. Frank, B. S., Vardar, D., Chishti, A. H., and McKnight, C. J. (2004) The NMR structure of dematin headpiece reveals a dynamic loop that is conformationally altered upon phosphorylation at a distal site. *J. Biol. Chem.* **279,** 7909–7916
19. Jiang, Z. G., and McKnight, C. J. (2006) A phosphorylation-induced conformation change in dematin headpiece. *Structure* **14,** 379–387
20. Chen, L., Jiang, Z. G., Khan, A. A., Chishti, A. H., and McKnight, C. J. (2009) Dematin exhibits a natively unfolded core domain and an independently folded headpiece domain. *Protein Sci.* **18,** 629–636
21. Uversky, V. N., Gillespie, J. R., and Fink, A. L. (2000) Why are "natively unfolded" proteins unstructured under physiologic conditions? *Proteins* **41,** 415–427
22. Vacic, V., Uversky, V. N., Dunker, A. K., and Lonardi, S. (2007) Composition Profiler: a tool for discovery and visualization of amino acid composition differences. *BMC Bioinformatics* **8,** 211
23. Vardar, D., Chishti, A. H., Frank, B. S., Luna, E. J., Noegel, A. A., Oh, S. W., Schleicher, M., and McKnight, C. J. (2002) Villin-type headpiece domains show a wide range of F-actin-binding affinities. *Cell Motil. Cytoskeleton* **52,** 9–21
24. Brown, J. W., and McKnight, C. J. (2010) Identifying competitive protein antagonists for F-actin with reverse-phase HPLC. *Anal. Biochem.* **398,** 117–119
25. Husain-Chishti, A., Levin, A., and Branton, D. (1988) Abolition of actin-bundling by phosphorylation of human erythrocyte protein 4.9. *Nature* **334,** 718–721
26. Marley, J., Lu, M., and Bracken, C. (2001) A method for efficient isotopic labeling of recombinant proteins. *J. Biomol. NMR* **20,** 71–75
27. Pardee, J. D., and Spudich, J. A. (1982) Purification of muscle actin. *Methods Cell Biol.* **24,** 271–289
28. Schuck, P., and Rossmanith, P. (2000) Determination of the sedimentation coefficient distribution by least-squares boundary modeling. *Biopolymers* **54,** 328–341
29. Vistica, J., Dam, J., Balbo, A., Yikilmaz, E., Mariuzza, R. A., Rouault, T. A., and Schuck, P. (2004) Sedimentation equilibrium analysis of protein interactions with global implicit mass conservation constraints and systemic noise decomposition. *Anal. Biochem.* **326,** 234–256
30. Brown, J. W., Vardar-Ulu, D., and McKnight, C. J. (2009) How to arm a supervillin: designing F-actin binding activity into supervillin headpiece. *J. Mol. Biol.* **393,** 608–618
31. Oda, T., Iwasa, M., Aihara, T., Maéda, Y., and Narita, A. (2009) The nature of the globular- to fibrous-actin transition. *Nature* **457,** 441–445
32. Pettersen, E. F., Goddard, T. D., Huang, C. C., Couch, G. S., Greenblatt, D. M., Meng, E. C., and Ferrin, T. E. (2004) UCSF Chimera: a visualization system for exploratory research and analysis. *J. Comput. Chem.* **25,** 1605–1612
33. Persistence of Vision Pty. Ltd. (2004) *Persistence of Vision Raytracer*, version 3.6, Persistence of Vision Pty. Ltd., Williamstown, Victoria 3016, Australia
34. Fischer, H., Polikarpov, I., and Craievich, A.F. (2004) Average protein density is a molecular weight-dependent function. *Protein Sci.* **13,** 2825–2828
35. Siegel, D. L., and Branton, D. (1985) Partial purification and characterization of an actin-bundling protein, band 4.9, from human erythrocytes. *J. Cell Biol.* **100,** 775–785
36. Husain-Chishti, A., Faquin, W., Wu, C. C., and Branton, D. (1989) Purification of erythrocyte dematin (protein 4.9) reveals an endogenous protein kinase that modulates actin-bundling activity. *J. Biol. Chem.* **264,** 8985–8991
37. Schuck, P., Perugini, M. A., Gonzales, N. R., Howlett, G. J., and Schubert, D. (2002) Size-distribution analysis of proteins by analytical ultracentrifugation: strategies and application to model systems. *Biophys. J.* **82,** 1096–1111
38. Azim, A. C., Knoll, J. H., Beggs, A. H., and Chishti, A. H. (1995) Isoform cloning, actin binding, and chromosomal localization of human erythroid

dematin, a member of the villin superfamily. *J. Biol. Chem.* **270,** 17407–17413
39. Volkmann, N., DeRosier, D., Matsudaira, P., and Hanein, D. (2001) An atomic model of actin filaments cross-linked by fimbrin and its implications for bundle assembly and function. *J. Cell Biol.* **153,** 947–956
40. Hampton, C. M., Liu, J., Taylor, D. W., DeRosier, D. J., and Taylor, K. A. (2008) The 3D structure of villin as an unusual F-actin crosslinker. *Structure* **16,** 1882–1891
41. Dyson, H. J., and Wright, P. E. (2005) Intrinsically unstructured proteins and their functions. *Nat. Rev. Mol. Cell Biol.* **6,** 197–208
42. Wright, P. E., and Dyson, H. J. (2009) Linking folding and binding. *Curr. Opin. Struct. Biol.* **19,** 31–38
43. Fink, A. L. (2005) Natively unfolded proteins. *Curr. Opin. Struct. Biol.* **15,** 35–41
44. Kim, A. C., Peters, L. L., Knoll, J. H., Van Huffel, C., Ciciotte, S. L., Kleyn, P. W., and Chishti, A. H. (1997) Limatin (LIMAB1), an actin-binding LIM protein, maps to mouse chromosome 19 and human chromosome 10q25, a region frequently deleted in human cancers. *Genomics* **46,** 291–293